Investigating the Wettability and Grain Surface Roughness of an Unconventional Oolitic Carbonate Reservoir

*Taiba Al-Wuhaib[1], Salah Almudhhi[1], Waleed Al-Bazzaz[2, *], Sohaib Kholosy[2], Saleh Al-Sayegh[3,4], Ralph Flori[3], Hasan Al-Saedi[5,6]*

[1]Kuwait University, Department of Petroleum Engineering, Sabah Al Salem University City, Kuwait.
[2]Kuwait Institute for Scientific Research, Petroleum Research Center, Ahmadi, Kuwait.
[3]Missouri University of Science and Technology, Rolla, Missouri, USA.
[4]Kuwait Oil Company, Ahmadi, Kuwait.
[5]Al-Amarah University College, Department of Petroleum Engineering, Maysan, Iraq.
[6]Missan Oil Company, Ministry of Oil, Iraq.

Abstract. Mineral surface roughness, or “roughness,” is a key factor in contact angle wettability estimates. In conventional studies, fluid-rock contact-angle surfaces are usually smoothed, polished, fluid-cleaned, and further aged using artificially impregnated reservoir fluids. Under these assumptions, smoothing the Oolite grain-surface sample alters the ooids' native conditions in this unconventional carbonate rock, leading to inaccurate wettability estimates. Unconventional Oolite contact-angle wettability measurements are sensitive to grain-surface roughness. Contact angles are measured at surfaces along the edges of its grain/pore systems. The integrity of the oolite sample, a crucial aspect, must be maintained to ensure it remains fresh, intact, and saturated with original reservoir fluids, as the nature of oolite grains introduces a noticeable tolerance for contact-angle error. The technique used in this study consumes low energy and is also fast in generating accurate wettability-preference data. The approach model for this contact angle correction (Tolerance Level) will be generated from extensive statistical data using 2D digital imaging technology. The study will use digital characterizations of both contact angles and grain/ pore surface roughness. The digital approach will cover capturing images of the Oolitic carbonate reservoir rock fabric, followed by two processing techniques: one for measuring the wettability contact angle and the other for measuring grain/pore surface roughness. The primary objective of this study is to characterize the wettability of the unconventional carbonate Oolite, including grain and pore surface roughness, contact angles, and reservoir rock petrophysics.

1 Introduction

This research aims to improve the accuracy of wettability measurements using a low-energy technology, which is crucial for rapid decision-making in secondary and tertiary advanced oil recovery programs in the oil and gas industry. Unconventional carbonate reservoirs, such as those with oolitic calcite mineral grain surfaces (Ooids), are not smooth, which affects conventional dynamic laboratory measurements of reservoir wettability [1-5,6-8, and 9]. Wettability is an essential factor governing the localization, velocity, and distribution of fluids within porous media and is influenced by the permeability of the surrounding environment [10]. Reservoir wettability is best preserved when measuring relative permeability using cores under original reservoir conditions [11 and 12]. However, tests on cores with altered wettability, such as cleaned cores or those contaminated with drilling mud surfactants, can lead to significant errors [13-16].

Knowing the accurate wettability preference and its detailed distribution in the reservoir will assist in selecting the optimized recovery treatment using the Al-Bazzaz wettability scheme [17-18, 1-2, 3-5, 6-8, 11]. The conventional method of measuring wettability via contact angle should be improved because it is not representative of complex reservoirs and is challenging to use for maintaining wettability while mimicking real reservoirs in processes that rely on artificial standard laboratory methods [19, 13, 20, 10, and 21]. Manipulation experiment-process environment modifications impose limitations on accuracy and, in most cases, do not account for the “Roughness” of unconventional calcite minerals available in the Oolitic mineral grain surfaces used in this study [19,3-4,13,14,22-24,10,25,21,9,26, and 37].

The assumptions (situation and method) need to be improved because the conventional method for measuring wettability relies on rough particle surfaces in carbonate

* Corresponding author: wbazzaz@hotmail.com

reservoirs dominated by the calcite Oolitic mineral. For grain surfaces that are not smooth, “Surface Roughness,” this study will bridge the gap of knowledge by linking rough Ooids’ mineral grain surface that inherits various textural ooids “peak” shapes and sizes, as well as surrounding complex “valley” pores, with reservoir wettability amid measuring statistical image wettability contact angle [3,27,28-29, 24,31,42,32,34-35,36,26, 44, and 58].

Rough Oolitic calcite mineral surfaces are captured using a Scanning Electron Microscope with Backscattered Secondary Electron Detectors (SEM-BSE) [12]. The captured images/frames will then be further examined using A.I.-based imaging methods. The associated 2D imaging processing technology will measure the wettability contact angle on the rough surfaces of Oolitic mineral grains in the Kuwaiti carbonate reservoir. This study will review the feasibility of producing complete regions of contact angle distribution measurements on the natural rough surfaces of Oolitic calcite and surrounding pores, thereby increasing confidence in the generated representation [1-2, 38-39, 3-6, 11, 40, 22, 30, 24, 41, 32, 42, 60 and 61].

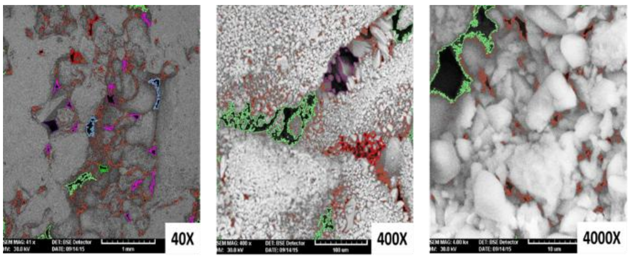

Fig. 1. The oolitic calcite unconventional rock sample is kept intact to preserve the surface grain roughness and the pore/ wall boundary contact angle network [3].

The accuracy of wettability measurement representation is achieved through the following steps: First, study the impact of rough mineral grain surfaces on wettability measurements [32]. Second, examine the concept of wettability, contact angle, roughness, and its effect on the real reservoir wettability [4-5]. Third, determine whether it is possible to obtain a complete contact angle measurement within the grain/pore system in the presence of a rough Oolitic calcite mineral grain surface [7-8]. Fourth, imaging methods, such as 2D imaging technology, can be used to quantify wettability. Finally, the study is limited to a specific carbonate reservoir in Kuwait [3].

This study evaluates the wettability preference of Oolitic fresh core plug(s) from a native Kuwaiti reservoir. This Oolitic calcite formation hosts hundreds of spherical grains (ooids) with thousands of pore shapes. Thousands of tortuous pore/ grain-wall boundaries and their subsequent shapes are captured, of which boundary geometry, size, and distribution are processed in an Oolite matrix image format (Fig. 2) [6].

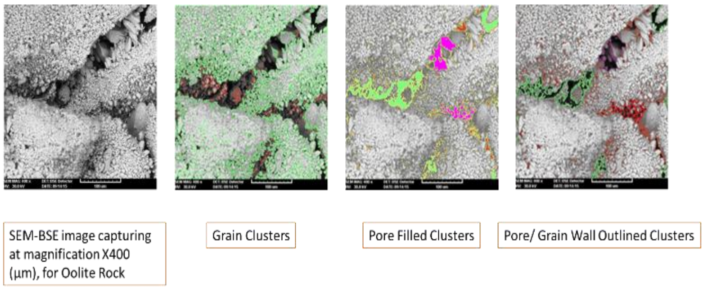

Figure 1 Based on the wettability measurement presentation, accuracy includes Oolitic grain surface cluster analyses, pore-filling cluster analyses, and pore/ grain wall outline cluster Analyses [3].

What is wetting? Wetting is the ability of a liquid to maintain contact with a solid surface, arising from intermolecular interactions between the two when they are brought together. The degree of wetting (wettability) is determined by a force balance between adhesive and cohesive forces [49]. Wettability affects relative permeability because it significantly controls the location, flow, and distribution of fluids in porous media, whether uniformly or fractionally wetted; water's relative permeability increases, and oil's decreases as the system becomes more oil-wet [11].

According to Al-Bazzaz et al. (2018) [21], a new classification of captured and measured contact angles is established: Strongly Water-Wet (SWW), Medium Water-Wet (MWW), Medium Oil-Wet (MOW), and Strongly Oil-Wet (SOW). According to Almudhhi et al. (2021), wettability in natural reservoir rocks is considered a distribution rather than a single value. Almudhhi et al. (2021) also introduced novel mirror-angle scenarios for wettability contact angles. All reservoirs have a unique signature of eight contact-angle classification regions, but in different proportions (Almudhhi et al., 2019). This knowledge will help us appreciate the potential success of heavy oil recovery using planned EOR and IOR techniques to improve recovery efficiency [1-2,38-39,4-8, and 11].

A new wettability classification is based on contact angles derived from big data. Seventeen classes show the degree of wetness preference that each pore area or pore/ grain boundary can possess [3].

In Figure 3, “Surface Roughness” (Ra) can be regarded as a measure of how far a surface deviate from smoothness, and it is hence linked to human perception of localized deviations from a normalized, perfectly flat plane [14 and 45]. From a mathematical perspective, it is related to the spatial variability structure of surfaces and, inherently, is a multiscale property, as the Ooid spheres on the calcite grain particle create uneven growth. The size of Ooids and the pores available on the surface plane will vary along the x-, y-, and z-axes, making surface contact with fluids a complex phenomenon. This complexity is governed by three processes: oil-water absorption on the rough surface, oil-water adherence (friction forces) on the rough surface, and the oil-water wetting preference on the rough surface. This study will focus only on the relationship between “Surface Roughness” and wettability preference, as measured by the contact angle (Hebbar [24]).

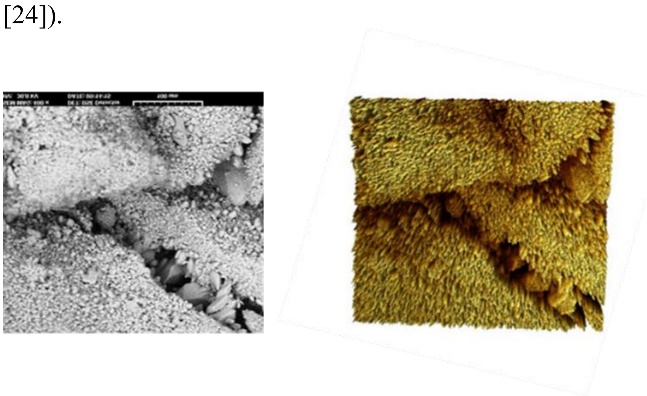

Fig. 3. (Left) SEM-BSE image capturing at magnification X400 (μm) for Oolite Rock. (Right) Roughness (Ra) image processed, SEM-BSE Image analyzed using SPM, an SPM Data Visualization and Analysis Tool

The surface structure of a solid element significantly affects and undermines the wettability of the same solid. A rougher surface has a lower wettability rate, while a less rough surface has a higher wettability capacity. The wettability of a rough surface is significantly affected by Wenzel factors, which are closely related and therefore warrant a discussion of the specific factors that influence wettability. No single factor can independently explain the wettability of rough surfaces, but the factors interrelate to define how wettability occurs. Researchers and scientists working on wettability and the Wenzel factors highlight the role of surface roughness reduction in enabling wettability [27, and 46-48].

1.1. Statement & Application

This groundbreaking study delves into the complex world of the carbonate Oolite calcite mineral grain surface, a rough surface within the pore that dramatically affects the measured reservoir wettability. We aim to determine whether it is possible to produce the remaining oil from an unconventionally measured contact angle within the microscopic grain/pore system in the presence of a rough mineral grain surface, such as this unconventional carbonate Oolite calcite. This unique and unconventional Kuwaiti carbonate reservoir presents a challenge we are eager to investigate, as accurate estimation of wettability is essential for forecasting enhancements in secondary and tertiary oil recovery [23].

1.1.1 Why does the conventional wettability method need to be improved?

Calcite/Oolite mineral grain surfaces are not smooth but rugged and complex in their wettability distribution. They can be measured on conventional, ideal 1D, mechanically prepared rock surfaces under controlled lab temperatures and manipulated fluid concentrations. Such conventional measurements, if performed, will yield an imperfect forecast of oil recovery. However, quantifying wettability contact angles using imaging methods (associated with 2D imaging technologies) is a practical, more accurate approach to managing oil production in this complex, unconventional reservoir with controlled mineralogy. The study will also recommend Oolite recovery charts to avoid unnecessary, expensive recovery treatments for future proven and recoverable unconventional Oolite oil [49-51,13-14,45,52-54, and 55].

1.1.2. What do we not know about unconventional carbonate Oolite mineral grain surface roughness, wettability, and contact angle?

Notably, the wettability contact angle roughness concept is poorly understood and, most notably, not measured in conventional lab tests. However, it can be estimated accurately using empirical formulas, partial models, or theoretical equations, as these unconventional reservoir rocks are far from actual conditions [38 and 39].

In this pioneering research study, we adopt a deterministic, microscopic approach to characterizing wettability and grain surface roughness. This approach is based on measuring the rough edges of ooids spread on the calcite grain surface, the surface contact angle at the boundary between the oolitic calcite grain surface and the adjacent pores, and the distribution of natural reservoir rocks. This novel approach allows us to delve deeper into the intricacies of wettability and surface roughness, providing a more comprehensive understanding of the relationship between surface roughness, wettability, and contact angle.

A wettability-morphological (geometrical) approach to capturing 2D images is critical for providing wettability mapping of pore geometry and contact angle that includes all Ooid shapes and sizes [56,17-18,1-2,32,39, and 23-24].

Moreover, the transformation of these pores and grains, mapped using big-data statistics into new definitions and newly measured (quantified) internal parameters, will not only lead to the discovery of Wettability contact angle distributions inside opaque core samples but also provide a practical tool. This tool has the potential to revolutionize our understanding of EOR distribution across fundamental reservoir rock properties, leading to more efficient and cost-effective recovery methods [56,38-39,3,6,8, and 11]. Introduce the Wettability contact angle relationship from the standpoint of rough-grained surface effects.

1.1.2 Past Digital Wettability Publication History

The digital wettability measurement study proposes a novel two-dimensional SEM–BSE imaging approach, combined with an AI-based clustering method, to estimate several complex carbonate reservoirs wetting preferences by quantifying large-scale contact angles through direct visual and statistical analyses. The digital wettability methodology has also been compared and validated against established techniques. Unfortunately, the only comparison is based on standard captive bubble or inverted sessile drop wettability measurement methods. Although the compared standard method involves direct experimental contact angle measurements, it does not capture real-world physics, such as grain morphology, grain-surface pore interactions, and surface roughness, and instead relies on an abstract, one-flat-surface mineral, no-pore effect, and limited laboratory data artificially manifested theory. These comparisons are nevertheless carried out in previous studies, as shown in Table 1.

Table 1. Past Digital Wettability Publication History

No.	Paper Title	Author (S)	Study Focus	Year	Publication Location	DOI
1	Characterization of Clay Minerals and Their Impact on Reservoir Permeability	Al-Bazzaz, W.H.	Nano Pores Characterization in Carbonates Using 2D SEM-BSE	2001	Thesis Of Master of Science, Socorro, NM. USA	
2	Impact of Clay Mineral Attributes in Estimating Damage in Carbonate Rocks	Al-Bazzaz, W. H. Al-Bazzaz, W.H., Engler, T.W.	Unconventional Nanopores in Jurrasic Carbontaes	2001-38	SCA, Edinburgh, Scotland	
3	Permeability Modeling Using Neural Network Approach for Complex Mauddud-Burgan Carbonate Reservoir	W. H. Al-Bazzaz, Y. Al-Mehanna, & A. Gupta	Neural Network Model for Complex Mauddud-Burgan Carbonate Reservoir	2007	SPE Middle East Oil and Gas Show and Conference	doi:10.2118/105337-ms
4	Porosity, Permeability, and MHR Calculations Using SEM and Thin-section Images for Characterizing Complex Mauddud-Burgan Carbonate Reservoir	W. H. Al-Bazzaz, Y. Al-Mehanna	Porosity, Permeability, and MHR Calculations Using SEM and Thin-section 2D Imaging: Scale and Field of View	2007	SPE, Asia Pacific Oil and Gas Conference and Exhibition	doi: https://doi.org/10.2118/110730-MS
5	INVESTIGATION OF NANO-POROSITY IN CARBONATE RESERVOIRS AND ITS ROLE IN UNDERSTANDING HYDROCARBON RESERVES AND RECOVERY ECONOMICS	Waleed Al-Bazzaz, Mohammad J Ali, and Misfera Al-Qahtani	Unconventional Nanopores in Carbontaes Potential and Economics	2008-54	SCA, 2008-54, Abu Dhabi, UAE	DOI: 10.5281/zenodo.6327812
6	Fracture Geometry Characterizations through Physical Modeling	z, W. H., Al-Tarkait, F., Ali, A., and M.	3D Fracture Physical Modeling on Core Plugs	2009	Kuwait International Petroleum Conference and Exhibition, Kuwait City, Kuwait,	https://doi.org/10.2118/127458-MS
7	3D seismic attribute analysis for structure and stratigraphy identification in Maui field, Taranaki Basin, New Zealand	A. Alhakeem, H. Almubarak, K. Liu, W. Al-Bazzaz	Thin-section 2D Digital Imaging Measurement	2017	New Zealand Petroleum Conference	
8	Up-Scaled Petrophysical Analyses Using Micro-Level Field-Of-View Petrographic Images for the Kapuni Group, Taranaki Basin, New Zealand	A. Alhakeem, K. Liu, W. Al-Bazzaz.	Up-Scaled Petrophysical Analyses Using Micro-Level Field-Of-View Petrographic Images	2017	AAPG 2017 Annual Convention and Exhibition, Houston, Texas, United States	
9	Investigating wettability contact angle measurement in Kuwaiti heavy oil reservoir and modeling using 2D imaging technologies	W. Al-Bazzaz, S. Almudhhi, & M. Alostath	Wettability Contact Angle Measurement Using 2D Imaging Technologies-Kuwaiti Reservoir	2018	SPE International Heavy Oil Conference and Exhibition	doi:10.2118/193706-ms
10	Investigating wettability contact angle measurement in Kuwaiti heavy oil reservoir and modeling using 2D imaging technologies	W. Albazzaz, S. Almudhhi & M. Alostath	Wettability Contact Angle Measurement Big Data Distribution	2019	PETROL SCI TECH-NOL. VOL. 37, NO. 6, 694–700	doi:10.1080/10916466.2018.1564767
11	Understanding O/G Shale Reservoir Tortuosity by Imaging Characterizations	Mohammad Sewailan, Waleed Al-Bazzaz	Shale Reservoir Tortuosity Measurements and Modeling by 2D Imaging Technology	2019	SPE Gas & Oil Technology Showcase and Conference, Dubai, UAE, October 2019.	https://doi.org/10.2118/198659-MS
12	An unconventional approach in investigating wettability contact angle measurement in shale resources	S. Almudhhi, M. Alostath, W. Al-Bazzaz, H. Sharifigaliuk, & A. Qubian.	Pore Morphology and Mineral Composition that control Shale wettability Preference	2021	PETROL SCI TECHNOL, Vol. 40, Issue 8, Pages 893-936	https://doi.org/10.1080/10916466.2021.2008969
13	Complexities Driving Wettability Evaluation of Shales toward Unconventional Approaches: A Comprehensive Review	Hamid Sharifigaliuk; Syed Mohammad Mahmood; Waleed Al-Bazzaz; Vahid Khosravi	Mineral Composition, Organic Matter Content, Generated Pore Types, Pressure, Temperature, and Saturation Conditions Relations to Observed Wetting Affinity.	2021	Energy & Fuels, Vol 35/Issue 2	doi:10.1021/acs.energyfuels.0c03661
14	Investigation of Pore Geometry Wettability Preference in an Oolitic Oil Reservoir: Pore Scale Imaging and Modelling Study	Al-Ajaj, Hussien, Ralph, Flori, Alsayegh, Saleh, Al-Mubarak, Haidar, Al-Bazzaz, Waleed	Complex Morphology of Oolitic Calcite Grains and Pores Wettability Preference	2022	The 35th International Symposium of the Society of Core Analysts, Austin, Tx. USA	DOI: 10.5281/zenodo.7087702
15	Are Natural Fractures in Sandstone Reservoir: Water Wet–Mixed Wet–Or Oil Wet?	Almudhhi, S., Abdullah, L., Al-Bazzaz, W.H., Alsayegh, S., Alajaj, H., Flori, R.	Inside Fracture, Fracture Wall Surface, and Adjacent Matrix Wettability Preference	2022	Journal of Engineering Research / Petroleum Engineering. Vol 11 No 1B	DOI: https://doi.org/10.36909/jer.17719
16	Practical Imaging Applications of Wettability Contact Angles on Kuwaiti Tight Carbonate Reservoir with Different Rock Types	Al-Sayegh, Saleh, Flori, Ralph, Al-Bazzaz, Waleed, Kholosy, Sohaib, Al-Saedi, Hasan, Abbas, Abdulaziz, and Ali Qubian	Unconventional Tight Carbonate Wettability Characterizations	2023	SPE, Gas & Oil Technology Showcase and Conference, Dubai, UAE	https://doi.org/10.2118/214165-MS
17	Practical imaging applications of wettability contact angles on Kuwaiti tight carbonate reservoir with different rock types	Al-Sayegh, Saleh, Flori, Ralph, Al-Bazzaz, Waleed, Kholosy, Sohaib, Al-Saedi, Hasan, Abbas, Abdulaziz, and Ali Qubian.	Digital Image Wettability Technology to Generate Relative Permeability Curves	2023	AIP Conference Proceedings 2809(1):030010	DOI: 10.1063/5.0145483
18	Investigating Pore Body, Pore Throat, Nano-Pore Wettability Preference in Several Unconventional Kuwaiti Carbonate Reservoirs	Al-Sayegh, Saleh, Flori, Ralph E., Alajaj, Hussain, and Waleed Hussien Al-Bazzaz	Wettability Preference in Several Unconventional Kuwaiti Carbonate Reservoirs	2023	SPE/IATMI Asia Pacific Oil & Gas Conference and Exhibition, Jakarta, Indonesia	https://doi.org/10.2118/215371-MS
19	Kuwaiti Carbonate Reservoir Oil Recovery Prediction Through Static Wettability Contact Angle Using Machine Learning Modeling	Al-Sayegh, Saleh, Flori, Ralph, Al-Bazzaz, Waleed Hussien, Al-Saedi, Hasan, Al-Kaouri, Mostafa, and Ali Qubian	Oil Recovery Prediction Through Static Wettability Contact Angle Using Machine Learning Modeling	2023	SPE/IATMI Asia Pacific Oil & Gas Conference and Exhibition, Jakarta, Indonesia	https://doi.org/10.2118/215260-MS
20	IOR Recovery-Dashboard for Unconventional Kuwaiti Tight Carbonate Reservoir: Study of Pore-Level Wettability Contact Angle	Al-Sayegh, R. Flori, B. Al-Hamad, A. Qubian, and W. Al-Bazzaz	IOR Recovery Prediction Dashboard for Tight Carbonate Reservoir: Study of Pore-Level Wettability Contact Angle	2023	European Association of Geoscientists & Engineers., IOR+ 2023, Oct 2023, Volume 2023, p.1 – 12.	https://doi.org/10.3997/2214-4609.202331019
21	Unconventional Modeling and Investigation of Natural Fracture Wettability Distributions in an Unconventional Tight Kuwaiti Carbonate Reservoir	S. Alsayegh, S. Kholosy, W. Al-Bazzaz, R. Flori, and H. Al-Saedi	Natural Fracture Wettability Distributions	2024	First EAGE Workshop on Advances in Carbonate Reservoirs from Prospects to Development, Apr 2024, Volume 2024, p.1 – 5	https://doi.org/10.3997/2214-4609.2024634036
22	Identifying Wettability Preference of Dolomite Rock Based on Pore/ Grain Contact Angle Using the SEM-BSE Technique	Al-Ajaj, H., Al-Bazzaz, W. H., Flori, R. E., Ibrahim, D. S., Alsayegh, S., and H. AlMubarak	Unconventional Dolomite Reservoir Wettability Preference Using 2D SEM-BSE	2024	The Mediterranean Offshore Conference, Alexandria, Egypt	https://doi.org/10.2118/223209-MS
23	Investigations on Unconventional Tight Carbonate Rock Cores by Low-Field Nuclear Magnetic Resonance Relaxometry	Ok, S., Al-Bazzaz, W. & Bahzad, D	Low-Field NMR Relaxometry	2025	Pet. Chem. 65, 57–71	https://doi.org/10.1134/S0965544124060124
24	Visual Understanding of Rock Wettability Distribution to Contact Angle Regions and Oil Displacement Patterns in the Silty Sand Reservoir via 2D Pore-Scale Modeling	Al-Ajaj, H., Al-Bazzaz, W., Flori, R., Alsayegh, S., AlMubarak, H., Ibrahim, D. S., and H. Al-Saedi	Complex Grain Architecture Reservoirs Wettability Preferences (Clays, Silt, and Sand)	2025	The Middle East Oil, Gas and Geosciences Show (MEOS GEO), Manama, Bahrain	https://doi.org/10.2118/227786-MS

1.2 Objectives

The primary objective of this study is to investigate the size and shape-driven static contact angle. Our unique approach involves analyzing digitally captured 2D images of boundaries between Ooid grains and pores from fresh cores, segmented using SEM-BSE. This approach allows us to generate high-quality images/ maps that are instrumental in our research.

In the abstract, the method counts complete contact angles observed at the pore area and the pore/grain-wall boundary system, which are scale-characterized at the pore body, pore throat, and nanopores present in these Oolitic core plugs. This approach will honor the rough surfaces provided by the Ooid's vast shapes and sizes.

However, contributions to pore-wall boundary contact angle, wettability performance, and recovery efficiency are also captured, measured, processed, and modeled. These boundaries will host Ooid peaks and pore valleys

It is crucial to comprehend the new physics that will advance reservoir characterization and production improvement. This understanding is necessary to model the static contact angle of the natural pore-wall boundary system, accounting for grain particle surface roughness.

2 Materials and Methods

2.1 Materials

2.1.1 General Unconventional Oolite Carbonate Reservoir Description

Oolite is a type of chemical carbonate sedimentary rock, primarily limestone (calcite) and, to a lesser degree, dolomite. Oolite consists of spherical ooids, often pearl-like, that create a rough, uneven fabric. Ooid pearls are found on the surfaces of calcite ooid grains, with large voids separating these rough oolite surface particles. These rough surfaces of calcite ooids are coated with laminated, rounded layers of calcite or dolomite that affect fluid-measured contact angles and, hence, ultimate oil recovery. Inadequate quantification of wettability will delay EOR oil production. Consequently, these rough ooid surfaces and their digital contact-angle attributes must be measured at grain-surface planes and adjacent pore spaces at micrometer-scale distances. Moreover, we hope to find a relationship between surface roughness (Ra) and wettability contact angle (θ˚) [3 and 4].

2.1.2 Sample Preparation

The prepared Oolitic Kuwaiti reservoir rock sample is a fragment selected from an original, uncontaminated core. This fragment is fresh and contains reservoir fluids. It is imaged and characterized for pore and grain area "roughness" and pore/grain wall-wettability contact angle. The contact angles are presented in 2D using SEM-BSE imaging techniques [1-2,4-5].

2.1.3 K-Means Clustering Machine Learning Algorithm Using Python Distributions

The generated images are quantified using a predefined k-means clustering approach. K-means clustering is a vector quantization method that partitions several thousand contact angle observations into K = 10 clusters. Each observation belongs to the cluster whose mean is nearest. This approach quantifies statistical wettability and contact angle preferences. The generated contact angle data is used to estimate the wettability classification. Each image captured at X40, 400X, and 4000X magnifications will be analyzed for matrix pore-body, pore/grain boundary, and nano-pore systems to ensure all possible wettability size classifications and to capture the distribution of matrix features [3, 6, and 8].

2.1.4 2D-SEM-BSE Macroscopic/ Microscopic Measurement Scale

The level of information is reported at three magnifications, X40 (mm), X400 (μm), and X4000 (nm), where the statistical wettability contact angle and distinct morphological feature(s) are closely examined (Fig. 4). Because big data are reported for each magnification, only one image will be shown as an example of the proposed methodology [18, 7, and 11].

Suppose grain particles and pore spaces in the nanometer (4000X), micrometer (400X), and millimeter (40X) ranges coexist within a single piece of rock. In that case, a process design must be developed that includes all dimensions of the rock microstructure, represents all grain particles and pore spaces, and captures the full range of wettability and surface roughness. Therefore, a two-dimensional (2D) approach has been proposed that integrates multiple digital rock images (frames) at different resolutions within the pore/grain network modeling framework (Fig. 6).

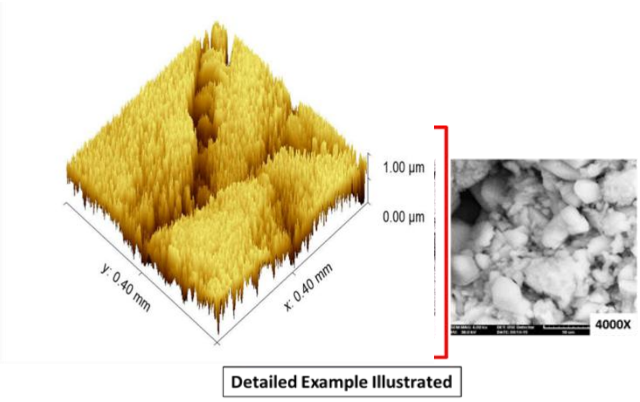

Fig. 4. The Minagish Oolite Sample Under Investigation, SEM-BSE Image Capture at Different Scales (40X, 400X, and 4000X) Showing the Surface Roughness. In this study, only 400X images will be illustrated for this study in detail [3].

In this study, we have used 2D-SEM-BSE imaging to understand the complex effects of wettability heterogeneity on contact angle classification regions at the pore scale by capturing images of an Oolite fragment at X40 (mm scale), X400 (μm scale), and X4000 (nm scale) in a rock sample. However, the example reported in this study will focus on image frames at X400 (micrometer scale). There are three image scales because the wettability contact angle can vary with the scale reported [8].

The SEM-BSE technique, a pivotal tool in our research, is used to capture images and measure morphological parameters. With its digital electron microscopy, this technique accurately measures several important morphological parameters of pore and grain spaces. These include grain surfaces, Ooid heights (peaks), conventional depths (valleys) of pore systems, and unconventional mineral systems such as Ooid shapes. Whether Ooid grain minerals, pore voids, or grain walls/pore voids boundaries, more geometrical parameters are captured, measured, and reported in a big data format. All available discrete pore areas, as well as all available discrete grain areas, their specific widths and specific lengths, shape elongations and shape roundness, and finally, their refracted contact angles and subsequent surface roughness, are reported explicitly.

2.2 2D Digital Angle Measurements Classification

The wettability classification in our research is based on the modern big-data clustering approach [3]. The static contact angle θ° is averaged to identify the wettability distribution in the pre-logic model, with values ranging from 0° to 360° [1-8]. The 2D-SEM technique is used for non-destructive imaging of core pores. A Kuwaiti Oolite fresh rock fragment sample is selected, and 2D pore/grain features are captured within a big-data quantification framework, which is then morphologically analyzed. Furthermore, these frames are modeled using unconventional grain/pore lengths with statistical artificial intelligence techniques (Fig. 5 and Table 1).

Fig. 5. Al-Bazzaz Wettability Contact Angle (Θ°) Classification Chart [12].

2.3 Oolite Quantitative Morphology Driven Wettability (θ˚) and “Roughness” (Ra) Investigation

Understanding the wettability of this unconventional Oolitic carbonate reservoir is complex, given the heterogeneity in grain size and mineral content across multiple scales. The complexity of the morphological features surrounding pore geometry further complicates contact-angle measurements. Hence, our research emphasizes the use of emerging technologies and unconventional approaches to better understand and characterize the wettability distribution of this unique rock, underscoring the depth and complexity of our work.

Three techniques are considered for quantifying the essential morphology of Ooid particles, the calcite grain particle “roughness,” and pore-filling surrounding the Ooids. First, the images under investigation are captured using scanning electron microscopy (SEM) with a backscattered electron imaging (BSE) system. Second, seven parameters directly associated with the captured Ooids/pore boundaries are measured. These parameters from SEM images are: pore counts; pore area (A) in μm2; pore perimeter (P) in μm; length (L) in μm; width (W) in μm; roundness (unitless); and elongation (unitless). The wettability contact angle (θ˚) is derived from a combination of big-data-reflected angles measured by backscattered electrons at the boundaries and A.I. clustering logics Almudhhi (2019) and Almudhhi (2021) [4-5]. Finally, a statistical image-processing technique is used to quantify the grain surface area in the same captured SEM images, measuring the surface roughness (Ra) in micrometers using data visualization and analysis from scanning probe microscopy (SPM) (Fig. 3 and Fig. 7).

Fig. 6. The Wettability vs. Surface Roughness Investigation of a Kuwaiti Carbonate Oolite: Study Scope of Work

2.3.1 Wettability Contact Angle (θ˚) Measurement

Digital styles were employed in this study to group measured contact angle and surface roughness data for the exact image/frame captured. This technology is limited to only 10 different color classes or clusters, as each measured cluster has a fixed color pattern. Therefore, the measured contact angle data can be spanned between 0° to 360° degrees over 10 clusters for each cluster, which is 36° degrees, as shown (Fig. 1, Fig. 2, and Fig. 5). These colors will clearly distinguish the images captured using the two-dimensional technology and assign a specific color to each cluster of the measured contact angles and surface roughness, making it easier to know the intensity of each cluster visually (Figures 1, 2, and 7).

Fig. 7. Wettability Contact Angle Classification Color Key Identification

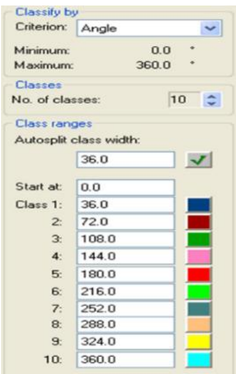

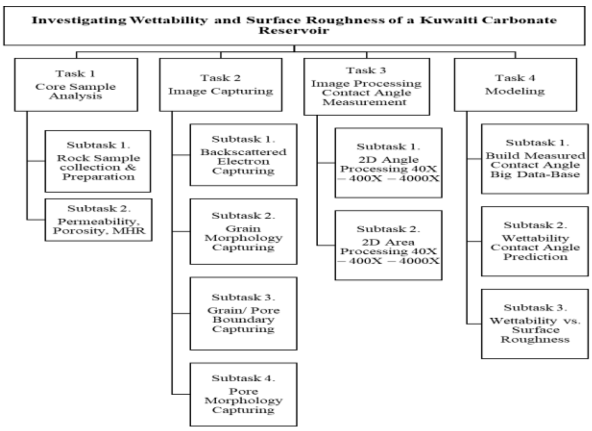

2.3.2 Grain and Pore Surface “Roughness” (Ra) SPM Measurements

The SEM image (frame) produced using the BSE method was also used in Scanning Probe Microscopy (SPM) software, and the following loading procedure was used. This meticulous process involved selecting the appropriate Z-scale, taking into account the sample's specific characteristics and the imaging system in use. A helpful starting point for the Z-Scale surface roughness is often the range of heights (0.5 µm peaks) or depths (0.5 µm valleys) present in the Oolite rock sample (totaling 1 µm). It is essential to consider the imaging system's limitations and adjust the Z-scale accordingly to maximize the visibility of features of interest, such as Ooids, without oversaturating the image or causing distortion (Fig. 8).

Fig. 8. SEM-BSE image captured at magnification X400 (µm) for Oolite Rock. The Oolite rock image is depth-processed and analyzed using an SPM Data visualization and analysis tool, with x=0.4 µm, y=0.4 µm, and z=1.0 µm.

The scanning probe microscopy (SPM) scan frame, with carefully selected axes, ensured that all roughed ooid peaks and all pore valleys captured in the frame image were included in the analyses. The meticulous masking process was then used to separate the grain-area feature from the pore area, enabling comprehensive analysis of surface roughness for each calcite particle with its unique and unconventional Ooid growth, thereby enhancing the research's thoroughness and completeness.

The researcher's active involvement in the masking selection process was not just a step but a crucial, integral part of our research. This process, when used to magnify rock specimens with SEM, was significant because it allowed us to isolate the area of interest in the image and ignore the surrounding background. By doing so, we could obtain a clearer view of the specimen's surface topography. The SPM tool then facilitated the easy application of the zone selection to the colored masked feature, effectively separating the area of interest from the surrounding background. The masking was applied seven times: four times for the grain particles and three times for the pore spaces. The mask's color was red (Fig. 11). This masking selection by the researcher was of utmost importance, as it enabled calculation of statistical quantities such as Surface Roughness Ra, RMS, volume, height, etc., using the software's statistical analysis tools (Table 3). Additionally, we could measure the remaining area more precisely by inverting the masked area (Fig. 9). Figure 9 shows an example of a masked calcite grain with Oolitic growth and pore areas. The two processing tools are applied: the image processing tool and the surface roughness SPM data visualization and analysis tool.

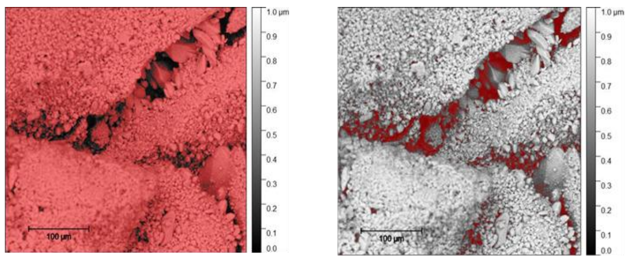

Figure 9 SEM-BSE images are processed and analyzed using a Scanning Probe Microscopy (SPM) data visualization and analysis tool. Masked areas are shown in red and represent the integrated areas studied; all analyses were carried out at the X400µm scale as an example representation of the method for surface roughness measurements. The left image shows a calcite

grain with Oolitic growth; hence, surface roughness statistical quantities are masked in that area. The right image shows statistical quantities of pore roughness in the masked areas.

Parameter	Description	Formula
R_a,	Arithmetic Average of Absolute Values	$Ra = \frac{1}{n}\sum_{i=1}^{n} \lvert y_i \rvert$
Rq, RMS	Root Mean Squared	$Rq = \sqrt{\frac{1}{n}\left(\sum_{i=1}^{n} y_i^2\right)}$
R_v	Maximum Valley Depth	$Rv = min_{y_i}$
R_p	Maximum Peak Height	$Rp = max_{y_i}$
R_t	Maximum Height of the Profile	$Rt = Rp + Rv$
R_{zk}	Skewness	$Rzk = \frac{1}{n \cdot R_q^3}\sum_{i=1}^{n} y_i^3$
R_{ku}	Kurtosis	$Rku = \frac{1}{n \cdot R_q^4}\sum_{i=1}^{n} y_i^4$
R_{zDIN}, R_{tm}	Average Distance between the highest peak and the lowest valley in each sampling length	$RzDIN = \frac{1}{s}\sum_{i=1}^{n} Rt_i$ [1]
R_{zJIS}	Japanese industrial standard Ra is based on the highest length and the lowest valley for the entire length	$RzJIS = \frac{1}{s}\sum_{i=1}^{n} Rt_i - Rv_i$ [2]

Table 2. The formulation of Models for Wenzel and Baxter Surface Roughness (Ra) and Approximations [6-8] provides a theoretical framework for our surface roughness measurements. These models, based on the work of Wenzel and Baxter, help us understand and interpret the surface roughness data we have collected from the Oolite rock.

[1] Where s is the number of sampling lengths.
[2] Rti and Rvi have the highest peak and lowest valley, respectively.

3 Results

Two sets of data have been yielded, one for wettability contact data (θ˚) and the second for surface roughness (Ra). Hundreds of thousands of data points are produced, and then several averages are applied to create the logic that exploits the relationship between (θ˚) and (Ra). An example of an unconventional carbonate Oolite for wettability and surface roughness investigations will be at the 400-micrometer scale, where pore throats and connectivity are clearly illustrated [58].

3.1 Unconventional Kuwaiti Oolite Rock Data Analysis

The routine core analysis of the sample under investigation, meticulously detailed in Table 3, confirms the oolitic carbonate and its calcite mineral description. The unconventional oolite mineral, with a porosity of 19.1% and a routine air-measured permeability of 966 mD, suggests excellent connectivity. This connectivity of pore spaces adds complexity and roughness to the lumpy oolite grain surface texture. The thoroughness and meticulousness of this data analysis provide a solid foundation for the conclusions drawn, instilling confidence in the findings.

The unconventionality of this carbonate reservoir is not solely due to its uneven pore geometry, size, or connectivity. It also stems from the unique, irregular, pearl-like spherical ooids that form unconventional relationships with the pore/grain wall. One such relationship concerns the interaction between the highly rough oolite grain surface and the resulting contact angle of wettability at the pore boundary [5-6, 56, and 13]. These unique and intriguing characteristics make the Oolitic carbonate reservoir a fascinating subject of study.

Table 3. The Petrophysics Routine Core Analysis for Unconventional Kuwaiti Oolite

Sample No.	Grain Density (gm/cc)	Ø (%)	K_{air} (mD)
T1	2.69	19.1	966

3.2 Wettability Contact Angle Data Analysis

In the BSE-SEM image (Figure 9 and Table 4), 2,229 Oolitic Ooids are captured at 400X magnification. These Ooids, when scanned across the 2,229 Ooids, have generated a massive amount of morphological big data [2], especially morphology scanned at the colored pores (Fig. 10b) as well as for Ooids grains (Fig. 10a). However, the wettability contact angle measurements, which are compared with the surface roughness analysis, are all yielded at the rough Oolitic grain surface adjacent to pores (Fig. 10c). The Ooids usually form at different sizes and spherical shapes. The surface roughness must be examined across several Oolitic grains and pores, which have tortuous textures and exhibit uneven parameters necessary for wettability investigations. As illustrated in Figure 4, only one scale is selected, 400X, with three measurement scans produced: wettability contact angle, grain clusters (10a), pore-filled wettability contact angle (10b), and finally, pore grain wettability contact angles (10c).

Fig. 10. Pore/Grain Wettability Contact Angle Clusters at X400 Magnification. (a) Wettability Contact Angle Grain Clusters. (b) Pore-Filled Wettability Contact Angle Clusters. (c) Pore/ Grain Wettability Contact Angle Outlined Clusters.

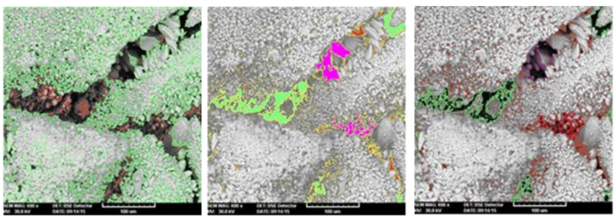

(a) (b) (c)

The unconventional Oolite sample at 400X magnification has 2,229 pore/grain-wall measurements over a mean area of 7,775 µm2. In this tiny area, 2,229 contact angles were measured, and the mean value is θ = 55.992°, or roughly 56° (Table 4). All 2,229 oolite features (grains, pores, and pore/grain boundaries) in the captured image have different lengths, widths, roundness, elongation, and diameters. The various shapes and sizes of these oolites will cause the unique surface roughness of the unconventional Oolite. According to Al-Bazzaz's classifications [18, 1-2, 38-39, and 49-50], this unconventional Kuwaiti carbonate Oolite oil reservoir is classified as 56˚, a medium-wet condition that is excellent for secondary water-flooding recovery [3-5, and 13].

Table 4. Captured and Measured All Ooids Morphological Adjacent Pore and grain area, contact angles for Unconventional rough surface at 400X (µm).

Total Pores Adjacent to Ooids	Area (µm2)	Perime-ter (µm)	Length (µm)	Width (µm)	Equiv. Diam-eter (µm)	Wettability Contact Angle (θ˚)
2,229 Pore Measure-ments						
Mean	7,775	43	2	1.32	0.32	56
Deviation	128	34.8	5.9	3	1.34	98.7
Minimum Pore	0.55	0	0.74	0.74	0	0
Maximum Pore	5,136	1,212.9	85.3	198.5	36.1	359.2

3.3 Oil Recovery Potential

According to Al-Bazzaz et al., the clustering of 2D measured contact angles (Table 1) (Fig. 5-7) can be transformed into a reservoir lifetime oil recovery potential scheme (Table 5) (Fig. 11). A deep machine learning post-logic predicts the type of recovery of this unconventional Oolitic reservoir rationed at the theoretical limit of oil volume yield at each reservoir type of recovery (Fig. 11). Types of recoveries will depend on logic-based primarily on digital wettability contact angle distribution (Fig. 5). The oil recovery potential model is based on 12 class system of contact angles (θ˚ Not including 0˚, 90˚, 180˚, 270˚, and 360˚), pore area, pore counts, and pore frequency (Table 1). The 5 previously mentioned angles were excluded from the model for the absence of a clear understanding of the physical and chemical status of liquid/ solid interactions.

Table 5 shows the simulated reservoir contact angle distributions in the 2D image captured at 400X magnification of the pore/grain map results, along with their corresponding theoretical recovery types. However, the overall average contact angle, based on 2229 pore measurements, is θ = 56° (Table 4). The average values suggest that this Oolite reservoir sample exhibits a medium water-wet (MWW) preference and is excellent for secondary water-flood recoveries. The model predicts strong water-wet (SWW) primary recovery of 13.3% oil, 6.7% medium water-wet (MWW) secondary water-flood oil recovery, weak water-wet (WWW) 19.6% low-salinity water flooding, weak oil-wet (WOW) 12.1% surfactant flooding, medium oil-wet (MOW) 7.9% polymer gel with high heat, and finally, strong oil-wet (SOW) 40.5% with unconventional high temperature > 300˚C. These results are summarized in Figure 11.

Table 5. The Type of Recovery Potential at 400X Magnification with Angle Pores θ˚ = 0˚, 90˚, 180˚, 270˚, and 360˚ are not included in the Wettability Contact Angle Predictive Model and Post logic Calculations.

Type of Recovery	Angle Range	Class	Std Average Area (µm²)	Std Avg Area's % Per Class	Pore Count Per Class	Pore Count %	Angle [θ˚]
Primary	0-30	1	13.669	5.87%	76	4.73%	16.4
Secondary	30-60	2	7.421	7.76%	144	8.96%	44.5
Low Salinity Water Flooding	60-90	3	3.505	14.43%	347	21.58%	87.3
Surfactant Flooding	90-120	4	11.880	6.86%	82	5.10%	106.4
Polymer Gel-High Heat	120-150	5	7.982	8.73%	142	8.83%	136.2
Water Flooding at High Temp.>300˚C	150-180	6	11.823	5.57%	99	6.16%	165.4
Water Flooding at High Temp.>300˚C	180-210	7	12.574	6.01%	80	4.98%	195.4
Polymer Gel-High Heat	210-240	8	7.610	9.07%	141	8.77%	224.1
Surfactant Flooding	240-270	9	4.968	18.42%	204	12.69%	263.8
Low Salinity Water Flooding	270-300	10	10.001	4.45%	73	4.54%	285.6
Secondary	300-330	11	9.102	6.68%	132	8.21%	315.1
Primary	330-360	12	11.806	6.13%	88	5.47%	344.7
Sum of values	0-360		112.341	100%	1608	100%	

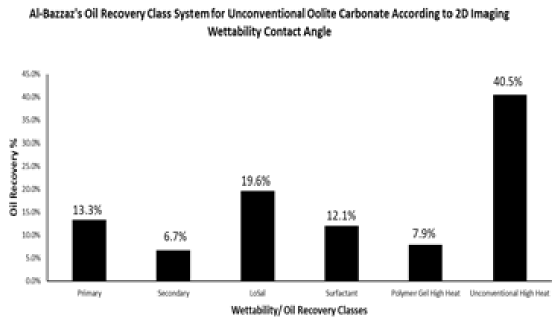

Fig. 11. Unconventional Oolitic Limestone Carbonate Reservoir Predictive Oil Recovery Model and logic-based primarily on Digital Wettability Contact Angle Distribution, 12 Class System of Contact Angles (θ˚ Not Including 0˚, 90˚, 180˚, 270˚, and 360˚), Pore Area, Pore Counts, and Pore Frequency.

3.4 Surface Roughness Data Analysis

The process of measuring surface roughness from BSE-SEM images involves two key features: the surface particles of the Oolite and the boundary between particles and pores. Figure 9 shows the masked red color on the oolitic particle's surface areas (left) and pore surface areas (right) between these particles. A 0.5µm depth height length is used to measure peak, and a 0.5µm depth length is used to measure valley thickness from the designed baseline axes (Fig. 12a- g).The roughness, which varies with the length between the top peak and bottom valley peak (1.0 µm band length; Figures 8 and 12 a-g), is then smoothed using the SPM tool, and the texture is produced (fig. 13).

The particles whose roughness is performed inside the 400X magnified image will be subdivided into seven group features of measurement surface roughness: A, B, C, D, E, F, and G. Four features, A, B, C, and D (Figure 12 a-d) will resemble the particle surface measurement and three features E, F, and G (Figure 12 e-g) will resemble the pore/ grain boundaries for the same image. Each subgroup has distinct measurements, confirming that the surface texture roughness of the oolite differs from that of Ooid grain particles and pore/grain boundaries (Tables 5-6).

3.5 Scanning Probe Microscopy (SPM) Data Visualization and Analysis

The 400X magnification image is captured and masked to highlight the necessary features (Fig. 12a-g). A statistical scan description test is carried out to ensure the reported surface roughness height (peak or valley) is sound and uninterrupted, given that the sensitive roughness (Ra) height is a projected measurement in micrometer lengths. SPM analyses use a series of moment-based and order-based quantifications on the masked area (Table 5). The scanning probe microscopy (SPM) analyses of Moment-based quantities are expressed using integrals of the height distribution function. SPM analyses of order-based quantities correspond to a specific ranking of maxima-peaks and minima-valleys along their median values (Table 5).

The one-dimensional surface texture is the calculated texture from two frequency components: a low-frequency waviness component and a high-frequency surface roughness component. This calculation is significant because it provides a comprehensive understanding of the surface shape and condition, including texture, by considering both peak and valley frequency components. The frequency depth at the surface roughness (high-frequency) is modeled for unconventional Oolite surface-roughness measurements. The SPM technique used to obtain the data is Scanning Probe Microscopy (SPM). Data processing involves statistical analysis of the SPM measurements. The measured peaks and valleys are sensitive to absolute roughness and thickness, with a detection limit on the nanometer scale. Tables 5 and 6 summarize the results.

Figure 12. The SEM-BSE image is meticulously processed and analyzed using a scanning probe microscopy (SPM) data visualization tool. The red-masked area, representing the integrated region analyzed, is a testament to the precision of our work. The example analysis illustrated is shown at X400 µm. Zones (A) in the left column are locations selected for Roughness (Ra) line-section analysis; the middle column shows locations within the masked area for Roughness statistical quantities analysis. The right column shows a Roughness profile chart, compared with Waviness and Texture, for each line section and masked area available in these images. Void surface grains are peaks: (a) Zone A. (b) Zone B. (c) Zone C. (d) Zone

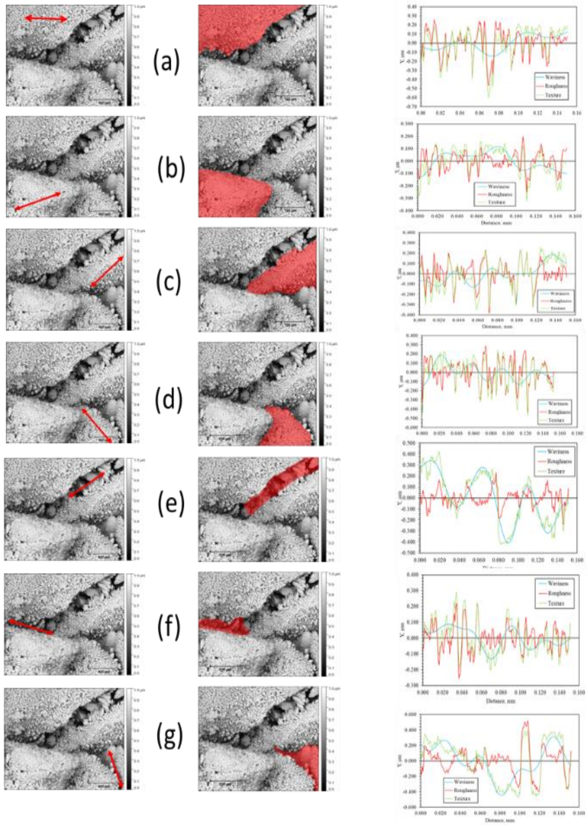

D. Pore spaces are valleys: (e) Zone E, (f) Zone F, and (g) Zone G.

Table 4. Our analysis is comprehensive, covering all aspects of the surface roughness. Statistical Quantities are calculated using the SPM-masked images. Zones A-D are Classified for Grain Roughness Statistics, and Zones E-F are Classified for

Pores Roughness. All Zones Represent the Entire Image Roughness (Ra).

Area of Classification	Zone A	Zone B	Zone C	Zone D	Zone E	Zone F	Zone G	All Zones
Moment Based								
Average Value (Ra), µm	0.674	0.725	0.638	0.657	0.415	0.33	0.532	0.63
RMS Roughness (Sq), µm	0.176	0.154	0.21	0.196	0.245	0.193	0.234	0.222
RMS (Grain-Wise). µm	0.176	0.154	0.21	0.196	0.245	0.193	0.234	0.222
Mean Roughness (Sa), µm	0.144	0.124	0.173	0.159	0.209	0.164	0.201	0.182
Skew (Ssk)	-0.646	-0.903	-0.612	-0.701	0.189	0.385	-0.249	-0.74
Excess Kurtosis	-0.08	0.491	-0.371	-0.113	-1.051	-0.835	-1.035	-0.24
Order-Based								
Minimum, µm	0.004	0.031	0	0	0	0	0	0
Maximum, µm	1	1	1	1	1	0.898	1	1
Median, µm	0.702	0.761	0.675	0.694	0.396	0.302	0.561	0.678
Maximum Peak Height (Sp), µm	0.326	0.275	0.362	0.343	0.585	0.568	0.468	0.37
Maximum Valley Depth (Sv), µm	0.671	0.694	0.638	0.657	0.415	0.33	0.532	0.63
Maximum Height (Sz), µm	0.996	0.99	1	1	1	0.898	1	1

Table 5. Surface Roughness analysis for masked zone sections: A-G of X400 (µm) SEM-BSE image sectioned zones. Zones E and F are roughness Ra for the pore sections of the image.

	Zone A	Zone B	Zone C	Zone D	Zone E	Zone F	Zone G
Roughness Average (Ra), µm	0.111	0.059	0.086	0.108	0.057	0.066	0.13
RMS Roughness (Rq), µm	0.145	0.073	0.114	0.134	0.076	0.084	0.17
Maximum Height of the Roughness (Rt), µm	0.726	0.449	0.616	0.725	0.471	0.477	0.91
Maximum Roughness Valley Depth (Rv), µm	0.468	0.251	0.382	0.433	0.237	0.257	0.39
Maximum Roughness Valley Height (Rp), µm	0.258	0.198	0.234	0.292	0.234	0.22	0.52
Average Maximum Height of the Roughness (Rtm), µm	0.55	0.304	0.467	0.515	0.323	0.298	0.50
Average Maximum Roughness Valley Depth (Rvm), µm	0.344	0.171	0.258	0.315	0.163	0.154	0.24
Average Maximum Roughness Peak Height (Rpm), µm	0.206	0.133	0.209	0.2	0.16	0.144	0.26
Average Maximum Height of the Profile (Rz), µm	0.592	0.317	0.521	0.629	0.328	0.343	0.60
Average Maximum Height of the Roughness (Rz ISO), µm	0.55	0.304	0.467	0.515	0.323	0.298	0.50
Maximum Peak to Valley Roughness (Rmax), µm	0.715	0.449	0.616	0.594	0.418	0.477	0.91
Skewness (Rsk)	-0.836	-0.377	-0.668	-0.447	-0.169	0.064	0.17
Kurtosis (Rku)	3.522	3.078	3.811	3.052	3.733	3.372	3.92
Waviness Average (Wa), µm	0.07	0.063	0.067	0.063	0.183	0.053	0.16
RMS Waviness (Wq), µm	0.08	0.069	0.086	0.079	0.217	0.061	0.20
Waviness Maximum Height (Wmax), µm	0.268	0.251	0.319	0.338	0.751	0.22	0.75

The parameter that merges moment-based and order-based features incorporates surface heights and spatial relationships and accounts for projected surface area. Additionally, it computes the volume as the integral of the surface height over the covered area, accounting for the mean inclination of the area's facets and representing the variation in surface slopes as waviness. Furthermore, it involves calculating the surface texture based on measured roughness (Ra) values and the moment-based and order-based surface roughness (Ra) calculations (refer to Fig. 13).

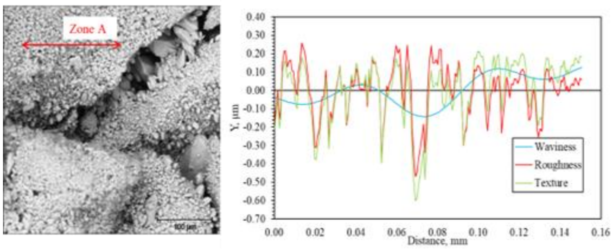

Fig. 13. Projected Roughness (Ra), Surface Waviness, and Simulated Texture for Grain particle of Zone A.

The summary results show the Roughness (Ra) at each selected masked zone area A-G, where grain particle zones A-D describe Zone A as 0.111 µm, Zone B at 0.059 µm, Zone C at 0.086 µm, and Zone D at 0.108 µm. In contrast, pore zones E-G describe Zone E at µm, Zone F at 0.066 µm, and Zone G at 0.131 µm (Fig. 14). The results shown in Figure 14 suggest that surface Roughness varies with grain and pore locations across the sample itself. These variations directly impact the total physical and chemical surface measurements, affecting whether wettability preference is measured using conventional techniques, the oil saturation distribution profile, or the relative permeability of these complex Oolite surfaces. These petrophysical properties change with variations in surface Roughness (Ra), directly affecting the projected recovery pattern. This is a significant finding that will shape future research in this field.

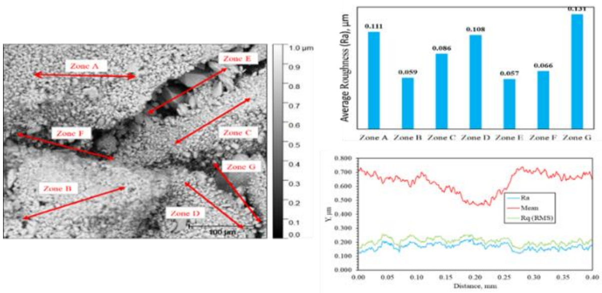

Fig. 14. Actual Surface "Roughness" for Both Grain Ooids and Pore Voids in the 400X sample Magnification. Zones A (Top Right) is the Peak and Valley height in Micrometers, and (Bottom Right) is the projected Y-height axis 2D Image Surface Roughness in Millimeters for the Captured Image.

4 Discussion

The SEM-BSE image is processed and analyzed using a scanning probe microscopy (SPM) with a data visualization tool. The red-masked area is the integrated region where all Roughness (Ra) and wettability analyses are successfully performed at a resolution of X400 µm. Zones A-D are for masked surface area roughness on the Oolite particles analysis section. Zones E-G are also for masked surface area roughness of the void's pore/ grain boundaries for the same Oolite sample at 400X. These seven representations successfully cover all Ooid grain particles and pore-space surface roughness, with the measured wettability contact angle distribution from the SEM-BSE (Table 7) at the exact locations integrated with the roughness analyses.

A 3D model of roughness is attempted using a frame (x = 0.4 mm, y = 0.4 mm, z = 1.0 µm) from the 400X Oolite carbonate sample. Ooid grain particle sample shows a uniform roughness in the sense of almost equal Ooid growth on the calcite mineral. Also, the roughness heights and widths are practically equal, suggesting that the ooid particle's roughness is homogeneous. This observation also suggests a calm and undisturbed precipitation environment for the mineral crystal. On the other hand, the pore/grain boundaries exhibit inconsistent roughness and unequal frequency lengths; hence, surface roughness at the boundaries is heterogeneous and significantly affects wettability.

The statistical roughness analysis (Table 7) shows that all seven zones are captured in the X400 Minagish Oolite. For zones A-D, the surface average roughness, Ra, is 0.111, 0.059, 0.086, and 0.108 micrometers, respectively. This result suggests that the ooid particle exhibits varying surface roughness, which affects the contact angle across the total surface. Even though the surface roughness is less than 0.2 µm, the particle's surface roughness will still influence its contact angle. The exact analytical surface roughness yield considers zones E-G for the pore/grain boundary, where Ra is 0.057, 0.666, and 0.131 µm, respectively. The maximum surface roughness (Ra) value is found in the pore zone G, 0.131 µm; the minimum surface roughness (Ra) value is found in the pore zone E, 0.057 µm. This observation suggests the diversity and heterogeneity of roughness at the pore/grain boundaries.

Table 7. Comparison between roughness on the Oolitic surface and roughness on the pore

	Roughness on Particle Zones (A+B+C+D)	**Roughness on Pore Zones (E+F+G)**
Roughness Average (Ra), µm	0.0.364	0.254
RMS Roughness (Rq), µm	0.466	0.336
Maximum Height of the Roughness (Rt), µm	2.516	1.864
Maximum Roughness Valley Depth (Rv), µm	1.534	0.888
Maximum Roughness Valley Height (Rp), µm	0.982	0.977
Average Maximum Height of the Roughness (Rtm), µm	1.836	1.122
Average Maximum Roughness Valley Depth (Rvm), µm	1.088	0.558
Average Maximum Roughness Peak Height (Rpm), µm	0.748	0.565
Average Maximum Height of the Profile (Rz), µm	2.059	1.278
Average Maximum Height of the Roughness (Rz ISO), µm	1.836	1.122
Maximum Peak to Valley Roughness (Rmax), µm	2.374	1.811
Skewness (Rsk)	-2.328	0.074
Kurtosis (Rku)	13.463	11.065
Waviness Average (Wa), µm	0.263	0.402
RMS Waviness (Wq), µm	0.314	0.48
Waviness Maximum Height (Wmax), µm	1.176	1.73

In Table 7, SPM-measured peaks and valleys represent real-space particle and pore roughness wavelengths. Particles on surface area Roughness (Ra) includes the roughness analyzed on the selected masked particles:

$$\text{Roughness Grain (Ra)} = A + B + C + D = 0.364\ \mu m \quad (1)$$

$$\text{Roughness Pore (Ra)} = E + F + G = 0.254\ \mu m \quad (2)$$

$$\text{Total Image Roughness, Ra} = \text{Particle} + \text{Pore} = 0.618\ \mu m \quad (3)$$

Particles on surface area Roughness (Ra) includes the roughness analyzed on the selected masked pores:

According to Table 8 and Figures 15, the study concludes that the wettability contact angle on the oolitic grains increases with magnification, indicating a direct proportionality described by y = 54.766 e0.147x and R2 = 0.9999. However, the wettability contact angle at the pore boundaries shows a weak relationship: it is inversely proportional, except at the pore throat (400X), which is the highest due to greater oil movement among the connected pores. Furthermore, the study concludes that surface roughness is directly proportional to magnification. The surface roughness is highest at the highest magnification, whether on the oolitic surface or surrounding pores.

Table 8. The wettability contact angle θ˚ of the Oolite grain and the surrounding pores versus surface roughness (µm) for the same feature across all investigated scales: 40X, 400X, and 4000X.

Magnification	Grain Wettability $(\theta^{\circ})_{Grain}$	Pore Wettability $(\theta^{\circ})_{Pore}$	Grain Roughness Ra (µm)	Pore Roughness Ra (µm)
40X	47.3	37.4	0.433	0.102
400X	40.8	55.2	0.642	0.049
4000X	35.3	32.5	0.689	0.227

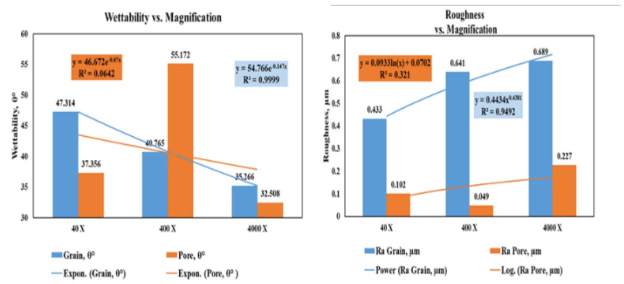

Fig. 15. (Left) Wettability relationship with magnification level from 40X to 4000X for grain and pore. (Right) Average Roughness relationship with magnification level from 40X to 4000X for grain and pore.

Moreover, the relationship between wettability and surface roughness is as follows: the higher the grain or pore surface roughness (Ra) in the unconventional Oolitic sample, the greater the water-wetting preference (θ˚), as shown in Figure 16.

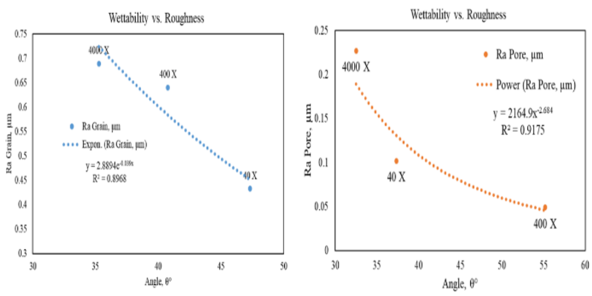

Fig. 16. (Left) Wettability Angle Relationship with Average Roughness at each magnification level for Grain. (Right) Wettability Angle relationship with Average Roughness at each magnification level for Pore.

Moreover, the relationship between the wettability and surface roughness is as follows: the more the grain or pore surface roughness Ra in the unconventional Oolitic sample, the more water wetting preference (θ˚). Figures 17.

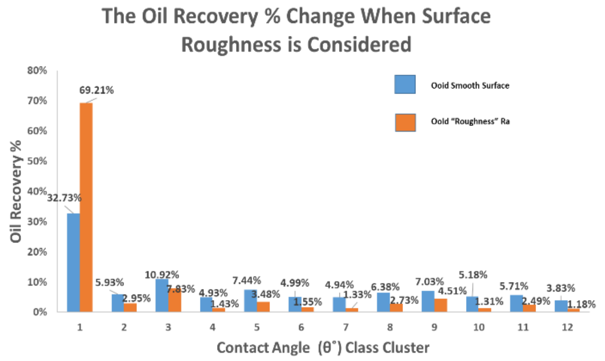

Fig. 17. Surface Roughness Error Tolerance Can Overestimate the Wettability Contact Angle Measurements during Mineral Sample Smoothing. This Error Will Lead to an Overestimate of Oil Recovery at the Planning Stage.

5 Conclusions

In conclusion, the majority of the ratio pore voids/grain walls, nano-pore size, and grain walls are Absolute-Strongly-Water-Wet (ASWW) close to θ = 10.2˚; however, insignificant indications of mixed and medium oil-wet conditions have been observed at the connecting pore throats, about θ = 56˚. To understand Oolite wettability, researchers must determine the entire distribution of core rock pore sizes at Nanometer, Micrometer, and Millimeter, their counts, and the morphology of the pore/grain-wall boundary, thereby indicating the wettability preference. This study also shows the importance of the uneven Oolitic carbonate surface grain minerals, their pore connectivity, contact angles, and crude oil recovery calculations and water production performance throughout the lifetime of the crude oil recovery phases of the Kuwaiti unconventional Oolite reservoir.

Surface roughness is directly linked to contact angle wettability, which integrates the effects of wettability on rough surfaces, as this Oolite demonstrates. Characterizations of wettability using contact angle measurements can capture roughness on both mineral grains and pore spaces, a task that was conventionally difficult and has led to less accurate wettability assessments in unconventional carbonate oil reservoirs. This study will consider Oolite carbonate reservoirs in Kuwait and apply 2D imaging technology with extensive data modeling methods.

At 400X (Micrometer Scale), the grain roughness is reported to be 0.642 µm, yielding a contact angle of θ = 40.2˚, while the conventionally measured grain surface, without any mention of surface roughness wettability, is θ = 56˚. There is a 15.8-degree reduction in contact angle, or 28.2%, making the oolite grain more wettable than it appears to be, which is favorable for more oil recovery and lower costs in future EOR treatment programs.

This study provides the oil industry with a summary of findings on surface-roughness wettability data, the EOR future outlook, and recommendations to understand the properties and importance of material surface roughness in relation to wettability for this oolitic carbonate reservoir. All wettability assessments are deterministic, with A.I. modeling emphasizing the quantification of surface roughness.

Acknowledgments
This study is submitted in partial fulfilment of the requirements for the degree of Master of Science in Petroleum Engineering at Kuwait University for Ms. Taiba Al-Wuhaib and her supervisor, Dr. Salah Almudhhi.

References

1. W.H. Al-Bazzaz, S. Almudhhi, M. Alostath, SPE-193706-MS, SPE Int. Heavy Oil Conf. and Exhib. (2018)
2. W.H. Al-Bazzaz, S. Almudhhi, M. Alostath, Pet. Sci. Technol. **37**, 694 (2019)
3. H. Al-Ajaj, R.E. Flori, S.H. Al-Sayegh, H. Al-Mubarak, W.H. Al-Bazzaz, 35th Int. Symp. of the Society of Core Analysts, Austin, TX (2022)
4. S. Almudhhi, M. Alostath, W. Al-Bazzaz, H. Sharifigaliuk, A. Qubian, Pet. Sci. Technol. **40**, 893 (2021)
5. S. Almudhhi, L. Abdullah, W.H. Al-Bazzaz, S. Al-Sayegh, H. Al-Ajaj, R.E. Flori, J. Eng. Res. **11** (2023)
6. S.H. Al-Sayegh, R.E. Flori, B. Al-Hamad, A. Qubian, W.H. Al-Bazzaz, EAGE IOR+ Conf., 1 (2023)
7. S.H. Al-Sayegh, R.E. Flori, H. Al-Ajaj, W.H. Al-Bazzaz, SPE-215371-MS, SPE/IATMI Asia Pacific Oil & Gas Conf., Jakarta (2023)
8. S.H. Al-Sayegh, R.E. Flori, W.H. Al-Bazzaz, H.N. Al-Saedi, M. Al-Kaouri, A. Qubian, SPE-215260-MS, SPE/IATMI Asia Pacific Oil & Gas Conf., Jakarta (2023)
9. H. Sharifigaliuk, S.M. Mahmood, W. Al-Bazzaz, V. Khosravi, Energy Fuels **35**, 1011 (2021)
10. T.M. Okasha, J.J. Funk, H.N. Rashidi, SPE-104496-MS, SPE Middle East Oil and Gas Show and Conf. (2007)
11. S. Al-Sayegh, R.E. Flori, S. Kholosy, W. Al-Bazzaz, H.N. Al-Saedi, A. Abbas, A. Qubian, AIP Conf. Proc. **2809**, 030010 (2023)
12. Y. Yuan, T.R. Lee, Springer Ser. Surf. Sci., 3 (2013)
13. M.B. Alotaibi, R. Azmy, H.A. Nasr-El-Din, SPE-129972-MS, SPE Improved Oil Recovery Symp. (2010)
14. H.N. Al-Saedi, S.K. Al-Jaberi, R.E. Flori, W.H. Al-Bazzaz, IPTC-19580-MS, Int. Petroleum Technology Conf., Dhahran (2020)
15. W.G. Anderson, J. Pet. Technol. **38**, 1125 (1986)
16. W.G. Anderson, J. Pet. Technol. **38**, 1246 (1986)
17. W.H. Al-Bazzaz, Y. Al-Mehanna, A. Gupta, SPE-105337-MS, SPE Middle East Oil and Gas Show and Conf. (2007)
18. W.H. Al-Bazzaz, Y. Al-Mehanna, SPE-110730-MS, SPE Middle East Oil and Gas Show and Conf. (2007)
19. W. Abdallah, J.S. Buckley, Oilfield Rev. **19**, 44 (2007)
20. E.R. Moldovan, C. Concheso Doria, J.L. Ocaña, L.S. Baltes, E.M. Stanciu, C. Croitoru, M.H. Tierean, Materials **15**, 2955 (2022)
21. M. Sewailan, W.H. Al-Bazzaz, SPE-198659-MS, SPE Gas & Oil Technology Showcase and Conf., Dubai (2019)
22. H.J. Deglint, C.R. Clarkson, C. DeBuhr, A. Ghanizadeh, Sci. Rep. **7**, 4347 (2017)
23. H.A. Hammood, A.K. Alhuraishawy, R.S. Hamied, W.H. Al-Bazzaz, SPE-198662-MS, SPE Gas & Oil Technology Showcase and Conf., Dubai (2019)
24. R.S. Hebbar, in *Membrane Characterization* (Elsevier, 2017), p. 219
25. R. Patel, R.K. Reddy Addula, M. Shaik, S.N. Punnathanam, J. Chem. Phys. **157**, 134705 (2022)
26. W. Wang, A. Gupta, SPE-30544-MS, 117 (1995)
27. U.M.K. Anwar, M.T. Paridah, A.S. Nordahlia, Y. Alia-Syahirah, H. Hamdan, S.H. Lee, J. Trop. For. Sci. **31**, 269 (2019)
28. Y. Ding, H. Geistlinger, Water Resour. Res. **57** (2021)
29. H. Gao, A.B. Tatomir, N.K. Karadimitriou, H. Steeb, M. Sauter, Adv. Water Resour. **157**, 104044 (2021)
30. A. Habibi, H. Dehghanpour, M. Binazadeh, D. Bryan, G. Uswak, SPE Reservoir Eval. Eng. **19**, 583 (2016)
31. G.J. Hirasaki, SPE Form. Eval. **6**, 217 (1991)
32. X. Huo, L. Sun, Z. Yang, J. Li, C. Feng, Z. Zhang, X. Pan, M. Du, Energies **16**, 7527 (2023)
33. S. Li, D. Dan, H.C. Lau, N.J. Hadia, O. Torsæter, L.P. Stubbs, SPE-196192-MS, SPE Annual Technical Conf. and Exhib. (2019)
34. E.R. Moldovan, C. Concheso Doria, J.L. Ocaña, L.S. Baltes, E.M. Stanciu, C. Croitoru, M.H. Tierean, Materials **15**, 2955 (2022)
35. H. Nakae, M. Yoshida, M. Yokota, J. Mater. Sci. **40**, 2287 (2005)
36. Ž. Pavlović, D. Risović, D. Novaković, Surf. Interface Anal. **44**, 825 (2012)
37. Y. Yuan, T.R. Lee, Springer Ser. Surf. Sci., 3 (2013)
38. A. Alhakeem, H. Almubarak, K. Liu, W. Al-Bazzaz, New Zealand Petroleum Conf., New Plymouth (2017)
39. A. Alhakeem, K. Liu, W. Al-Bazzaz, AAPG Annual Convention and Exhib., Houston (2017)
40. H.J. Deglint, C.R. Clarkson, A. Ghanizadeh, C. DeBuhr, J.M. Wood, J. Nat. Gas Sci. Eng. **62**, 38 (2019)
41. Y. Hu, SPE-173476-STU, SPE Annual Technical Conf. and Exhib., Amsterdam (2014)
42. A. Ivanova, A. Orekhov, S. Markovic et al., Sci. Rep. **12**, 1262 (2022)
43. K. Rykaczewski, T. Landin, M.L. Walker, J.H.J. Scott, K.K. Varanasi, ACS Nano **6**, 9326 (2012)

44. [AUTHOR NAME INCOMPLETE IN SOURCE] P. ...hoo, in *Mechatronics and Manufacturing Engineering* (Woodhead, 2012), p. 159
45. H.N. Al-Saedi, A. Qubian, W. Al-Bazzaz, R.E. Flori, IPTC-19740-MS, Int. Petroleum Technology Conf., Dhahran (2020)
46. B. Bhushan, J.C. Wyant, J. Meiling, Wear **122**, 301 (1988)
47. A.B.D. Cassie, S. Baxter, Trans. Faraday Soc. **40**, 546 (1944)
48. A.B.D. Cassie, Discuss. Faraday Soc. **3**, 11 (1948)
49. A.M. Alhammadi, A. AlRatrout, K. Singh et al., Sci. Rep. **7**, 10753 (2017)
50. A.K. Alhuraishawy, R.S. Hamied, H.A. Hammood, W.H. Al-Bazzaz, SPE-198666-MS, SPE Gas & Oil Technology Showcase and Conf., Dubai (2019)
51. A.K. Alhuraishawy, B. Bai, M. Wei, W.H. Al-Bazzaz, SPE-193763-MS, SPE Int. Heavy Oil Conf. and Exhib., Kuwait City (2018)
52. H.N. Al-Saedi, W. Al-Bazzaz, R.E. Flori, SPE-194820-MS, SPE Middle East Oil and Gas Show and Conf., Manama (2019)
53. H.N. Al-Saedi, R.E. Flori, S.K. Al-Jaberi, W. Al-Bazzaz, SPE-200488-PA, SPE J. (2020)
54. H.N. Al-Saedi, R.E. Flori, W. Al-Bazzaz, J. Mol. Liq. **306**, 112866 (2020)
55. A.K. Jaber, A.K. Alhuraishawy, W.H. Al-Bazzaz, SPE-198013-MS, SPE Kuwait Oil & Gas Show and Conf. (2019)
56. M.A. Al-Alwani, S. Dunn-Norman, L.K. Britt, H.H. Alkinani, A.T. Al-Hameedi, A.M. Al-Attar, H.A. Trevino, W.H. Al-Bazzaz, URTEC-198192, Asia Pacific Unconventional Resources Technology Conf., 995 (2019)
57. K. Chaudhary, M.B. Cardenas, W.W. Wolfe, J.A. Maisano, R.A. Ketcham, P.C. Bennett, Geophys. Res. Lett. **40**, 3878 (2013)
58. Y. Li, J. Yang, Z. Pan, W. Tong, Fuel **260**, 116352 (2020)
59. B. Zulfiqar, H. Vogel, Y. Ding, S. Golmohammadi, M. Küchler, D. Reuter, H. Geistlinger, Water Resour. Res. **56** (2020)
60. M. Andrew, B. Bijeljic, M.J. Blunt, Adv. Water Resour. **68**, 24 (2014)
61. M. Mahdaviara, M.N. Amar, M. Ostadhassan, A. Hemmati-Sarapardeh, Alex. Eng. J. **61**, 11601 (2022)